ORIGINAL ARTICLE

Effect of structural differences of pumice on synthesis of pumice-supported nFe^0: removal of Cr (VI) from water

Bilsen Tural[1] · Erdal Ertaş[1] · Mehmet Güzel[1] · Servet Tural[1]

Abstract

In this study, pumice from different regions of Turkey (Diyarbakir, Southeast Turkey and Bitlis, East Turkey) has been supplied and used as supporting material for nanoscale zero-valent iron (nFe^0). Native Bitlis pumice (NBP)-supported nanoscale zero-valent iron (BP-nFe^0) and native Diyarbakir pumice (NDP)-supported nanoscale zero-value iron (DP-nFe^0) were synthesized under the same conditions. Native pumice (NDP, NBP) and pumice-supported nFe^0 (DP-nFe^0 and BP-nFe^0) adsorbents were morphologically and structurally characterized by SEM, EDX, XRF and BET. When using NBP as support material, the iron content of the BP-nFe^0 increased 1.9-fold from 1.99 to 3.83%. However, iron content of NDP (2.08%) increased approximately 29 times after it is used as a support material in synthesis of DP-nFe^0 (60%). The removal potential of native pumice (NBP and NDP) and iron-modified pumice (BP-nFe^0 and DP-nFe^0) samples was investigated to remove Cr(VI) ions. The parameters of solution pH, initial metal concentration, contact time and the amount of adsorbent in the removal of chromium (VI) ions were investigated. Langmuir, Freundlich, Temkin, Dubinin–Radushkevich and Jovanovic isotherm models were used to evaluate the adsorption equilibrium data. The equilibrium adsorption was found so as to be well described by the Langmuir isotherm model for all the adsorbents studied. The maximum adsorption capacity of Cr(VI) ions for NDP, NBP, DP-nFe^0 and BP-nFe^0 was 10.82, 14.30, 161.29 and 17.39 mg/g, respectively. The rate of Cr(VI) removal was subjected to kinetic analysis using pseudo-first-order, pseudo-second-order, intraparticle diffusion and Elovich models. Kinetic studies suggest that adsorption of NDP, NBP, DP-nFe^0 and BP-nFe^0 described more favorably by the pseudo-second-order kinetic model. The results showed that NDP is a much better support material for nFe^0 when compared to NBP.

Keywords Pumice · Hexavalent chromium · Nano-zero-valent iron · Adsorption · Comparison

Introduction

Until recent years, water pollution caused by various pollutants such as dyes, heavy metals and toxic anions has been increasing rapidly due to industrial wastes thrown into the environment without treatment (Rangabhashiyam and Balasubramanian 2019a, 2018; Alam, 2014; Selvakumar and Rangabhashiyam 2019; Periyasamy et al. 2020). Heavy metals are extremely durable, bioaccumulative and inherently the most toxic (Rangabhashiyam and Balasubramanian 2019b). Among them, chromium (Cr) is one of the common heavy metals used in several metal surface treatment, electroplating, industrial processes, mining, chrome plating,

wood preservation, including metal processing and leather tanning (Wang et al. 2020; Rangabhashiyam and Balasubramanian 2018). The chromium mainly exits in the aquatic environment in two oxidation situations, that is, trivalent chromium Cr(III) and hexavalent chromium Cr(VI) with significant differences. Hexavalent chromium is more water soluble, less stable, easily enters living cell and more toxic than trivalent chromium (Huang et al. 2016). The harmful effects of Cr(VI) cause health problems in humans such as dermatitis, skin irritation, bleeding, epigastric pain, bronchitis, chronic ulcers, nasal septum perforation, lung cancer, pneumonia and liver inflammation (Rangabhashiyam and Balasubramanian 2019b).

The World Health Orgnization (WHO) and the US Environmental Protection Agency (USEPA) restricted their maximum contaminant level of total Cr(VI) in potable water as 0.05 and 0.1 mg/L, respectively (Rangabhashiyam and Balasubramanian 2018; Li et al. 2020). Consequently, it is

✉ Bilsen Tural
   bilsentural@gmail.com

1 Department of Chemistry, Faculty of Education, Dicle University, 21280 Diyarbakir, Turkey

an imperative aim to treat Cr-polluted wastewater previous to discharge so as to the environment (Liu et al. 2020). Various methods such as chemical precipitation, electrochemical treatment, biological methods, membrane separation, ion exchange and adsorptive methods have been used to separate heavy metals from wastewater (ALOthman et al. 2013; Sun et al. 2020; Deng et al. 2020; Qin et al. 2020; Liu et al. 2020). Adsorption among all the other methods studied, it has been one of the preferred methods for Cr(VI) removal due to its efficiency, operational simplicity and low cost (ALOthman et al. 2013). Conversely, other methods have many disadvantages, such as being uneconomical and incomplete removing Cr(VI), requiring high reactive and energy, and creating toxic sludge or other waste products that require disposal or treatment (ALOthman et al. 2013). However, the high cost of adsorbents is one of the biggest obstacles for industries to apply the adsorption process. The cheapness of adsorbents reduces the cost and increases the applicability of adsorption technology. Therefore, there is a need to develop low-cost and readily available adsorbents for the removal of Cr(VI) ions from aqueous media (ALOthman et al. 2013).

Recently, nFe^0 has been used to remove heavy metal impurities. nFe^0 has become one of the promising and effective technologies in the removal of substances in the environment due to its large surface area, high reactivity and very small particle size. nFe^0 is also capable of converting toxic substances into their non-toxic forms (Simeonidis et al. 2016; Jiang et al. 2018; Zhang et al. 2019). nFe^0 can also be used to promote the reduction and precipitation of toxic and carcinogenic metals such as Cr(VI) to more stable forms such as Cr(III) (Dalal and Reddy 2019). However, the reduction in reactivity and mechanical strength, as well as agglomeration, limited the application of nFe^0 when used in conventional treatment systems (Shu et al. 2020; Zhu et al. 2018). Furthermore, another problem is the difficult separation from the aqueous medium resulting from the small size of nFe^0. In recent years, this problem has been compensated by immobilization, fixation or confinement of nFe^0 to supporting materials such as silica, zeolite, kaolinite, bentonite, activated carbon, zeolites or polymer membranes. Immobilization of such materials, apart from the immobilization of nFe^0, also affected their physicochemical properties. Immobilization of nFe^0 also affected its physicochemical properties (Xu et al. 2018; Luo et al. 2019; Wu et al. 2020; Zhang et al. 2019). More importantly, the removal of adsorbent from the aqueous medium to remove water impurities through magnetic separation was strikingly advantageous by nFe^0. This method has significant advantages in terms of speed and time compared to other conventional methods (Li et al. 2017).

Pumice is a rock formed as a result of volcanic eruptions with a large surface area and a skeletal structure, including open channels that allow water and ions to enter and exit the crystal structure. It can also be easily processed in metal removal and can be used as a suitable material due to its low cost (Amin et al. 2018; Indah et al. 2018; Guler and Cebeci 2017). Pumice having basic and acidic character has a high silica content that makes a negatively charged surface. Reducing the negative charge on the surface of the pumice increases its adsorption capacity and therefore acidification is performed (Samarghandi et al. 2013; Derakhshan et al. 2013; Jonasi et al. 2017).

The main objectives of this study are structural analysis of NBP and NDP; synthesize and characterize NBP- and NDP-supported nFe^0 (BP-nFe^0, DP-nFe^0); use of NBP, NDP, BP-nFe^0 and DP-nFe^0 in the removal of Cr(VI) and determine and evaluate the adsorption efficiency under different experimental conditions; the use of magnetic separation method to separate BP-nFe^0 and DP-nFe^0 from aqueous media; comparison of Cr(VI) removal efficiencies of NBP, NDP, BP-nFe^0 and DP-nFe^0 adsorbents.

Materials and methods

Materials

The following chemical reagents were used: 1,5-diphenylcarbazide, $K_2Cr_2O_7$, $FeCl_3·6H_2O$, $NaBH_4$, HCl, NaOH and ethanol, which are all analytical reagent grade (Fluka, Sigma-Aldrich ve Merck). All chemicals were applied as delivered without further purification. As for support layer, pumice was supplied from different regions of Turkey. Native Diyarbakir pumice from Southeast Turkey and native Bitlis pumice from East Turkey were obtained and analyzed by X-ray fluorescence spectrometry (XRF, Rigaku ZSX Primus II). Native Diyarbakir pumice consisted of SiO_2—69.9%, Al_2O_3—12.6%, Fe_2O_3—5.29%, Na_2O—4.21%, MnO—0.159%, K_2O—6.48% and native Bitlis pumice consisted of SiO_2—63.7%, Al_2O_3—16.5%, Fe_2O_3—4.03%, Na_2O—0.933%, MnO—0.078%, K_2O—6.23%. To obtain 1000 mg/L aqueous stock solution of Cr(VI) for later use, 2.829 g of potassium dichromate ($K_2Cr_2O_7$) was dissolved in one thousand mL deionized water. In this study, the solutions with desired concentrations were attained by diluting with deionized water of the stock solution.

Preparation and characterization of DP-nFe^0 ve BP-nFe^0

Native Diyarbakir pumice from Southeast Turkey and native Bitlis pumice from East Turkey were ground to 45 μM and acidified with 1% HCl for 24 h. It was washed several times with deionized water so as to remove impurities and until pH reached neutral levels. Acid activated native Diyarbakir

pumice (NDP) and native Bitlis pumice (NBP) were dried at 65 °C in the oven and were prepared for nFe^0 coating (Guler and Cebeci 2017). The coating process was performed according to Liu et al. (2014). The NDP- and NBP-supported nFe^0 (DP-nFe^0 and BP-nFe^0) were produced according to conventional liquid phase method in which the pumice was used as a support layer and borohydride ($NaBH_4$) was used as a reduction agent for iron ions ($FeCl_3$) (Shi et al. 2011; Üzüm et al. 2009; Liu et al. 2014; Ponder et al. 2000). After 3.36 g of NDP and NBP was introduced into the three-necked flask, the iron solution obtained by dissolving 1.35 g of $FeCl_3.6H_2O$ in 100 mL of ethanol/water (8:1 ratio) was added and stirred under argon gas for 1 h. Then, $NaBH_4$ solution prepared by dissolving 0.95 g of $NaBH_4$ in 100 mL of purified water was added to the mixture at a drop rate of 60 drops per minute. The mixture was stirred in the sonicator for 2 min every 10 min. After the addition of $NaBH_4$ is complete, stirring was continued for one hour (Liu et al. 2014; Qasim et al. 2018). The synthesized composite is separated with a magnet and dried at lyophilizer (CHRIST, Alpha 2–4 LDplus). The theoretical mass fraction of the synthesized nFe^0 is 7.7% of pumice-supported nFe^0 adsorbents (Liu et al. 2014). The micromorphology features were observed by scanning electron microscopy (SEM, Quanta 400F). Elemental mapping was obtained by energy-dispersive X-ray spectroscopy (EDX, Jeol 2100F microscope). The surface areas of NDP, NBP, DP-nFe^0 and BP-nFe^0 adsorbents were measured using the BET-N_2 adsorption method (Brunauer–Emmett–Teller isotherm) using the Accelerated Surface Area and Porosimetry Analyzer (Micromeritics-TriStar II Plus 3030, USA).

Batch experiments

Batch experiment for Cr(VI) removal was carried out in 50 mL flasks at room temperature using the mechanical agitation (IKA@KS 4000i) at 200 rpm. Various experimental parameters such as adsorbent dose (2, 4, 6, 8, 10 g/L), initial pH (1–9), initial Cr(VI) concentration (25, 50, 75 mg/L) and contact time (1–90 min) were studied. All experiments were repeated three times. The solid and liquid phases are separated by a magnet. The determination of Cr(VI) in the supernatant was performed with a UV–Vis spectrophotometer (Agilent Cary 60) using a 1,5-diphenylcarbazide spectrophotometric method at 545 nm.

Results and discussion

Characterization

The results of the chemical composition of NBP, BP-nFe^0, NDP and DP-nFe^0 obtained from EDX (energy-dispersive

X-ray spectrophotometer) analysis are shown in Table 1. When the native pumice taken from different regions of Turkey was used as support material, although the synthesis method and conditions were the same, the amount of nFe^0 formed on the surfaces of the NDP and NBP was affected. Iron content, which was 1.99% in NBP, increased 1.9-fold after synthesis to 3.83%. The iron content of NDP and DP-nFe^0 is 2.08% and 60%, respectively, that is, the iron content increased 29 times after synthesis of DP-nFe^0. Harman and Ibrahim (2018) used the Isparta pumice with 2.03% iron content as a support material, and after the synthesis of P-nZVI, the iron content increased to 41.98%, that is, 21 times with the same synthesis method.

SEM images of NBP, BP-nFe^0, NDP and DP-nFe^0 are shown in Fig. 1. As seen in Fig. 1, NDP has an irregular or oval-shaped mesh of internal cavities/pores or vesicles, some of which are interconnected and open to the outer surface that provides suitable sites for adsorption compared to NBP. The images of DP-nFe^0 and BP-nFe^0 revealed that the prepared Fe^0 nanoparticles showed heterogeneous distribution on the pumice surface. The Fe^0 nanoparticles appear to be spherical in shape and do not have a single size. In the images of DP-nFe^0 and BP-nFe^0, when NDP was used as a support material, Fe^0 nanoparticles were formed much more on the surface. This is probably due to the morphological differences between NDP and NBP.

The specific surface area of adsorbents was measured using a BET-N_2 surface area analyzer. The average specific surface area of NDP and NBP natural pumice was measured as 6.3 and 1.3 m^2/g, respectively. The specific surface areas of DP-nFe^0 and BP-nFe^0 obtained by covering the surfaces of two native pumice with nFe^0 were measured as 40.5 and 6.8 m^2/g, respectively. nFe^0 coating of NDP, which has a larger surface area than NBP, has increased the surface area much more.

Influence of pH

The control of surface load in removing adsorbate from solution is significant, and the pH of the solution determines the surface charge. Due to the important role of pH in adsorption, the pH effect was examined in the range

Table 1 Elementary composition of NBP, BP-nFe^0, NDP and DP-nFe^0 from EDX characterization

Elements (wt%)	NBP	BP-nFe^0	NDP	DP-nFe^0
Al	5.77	4.89	8.16	4.40
Si	27.93	26.34	37.76	15.50
K	2.70	2.90	5.82	2.48
Fe	1.99	3.83	2.08	60

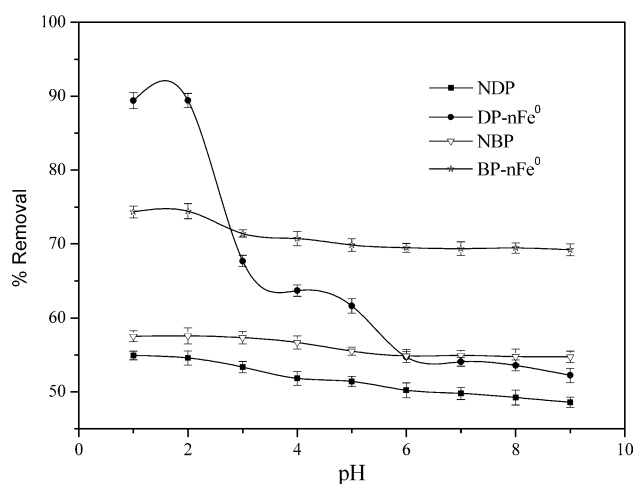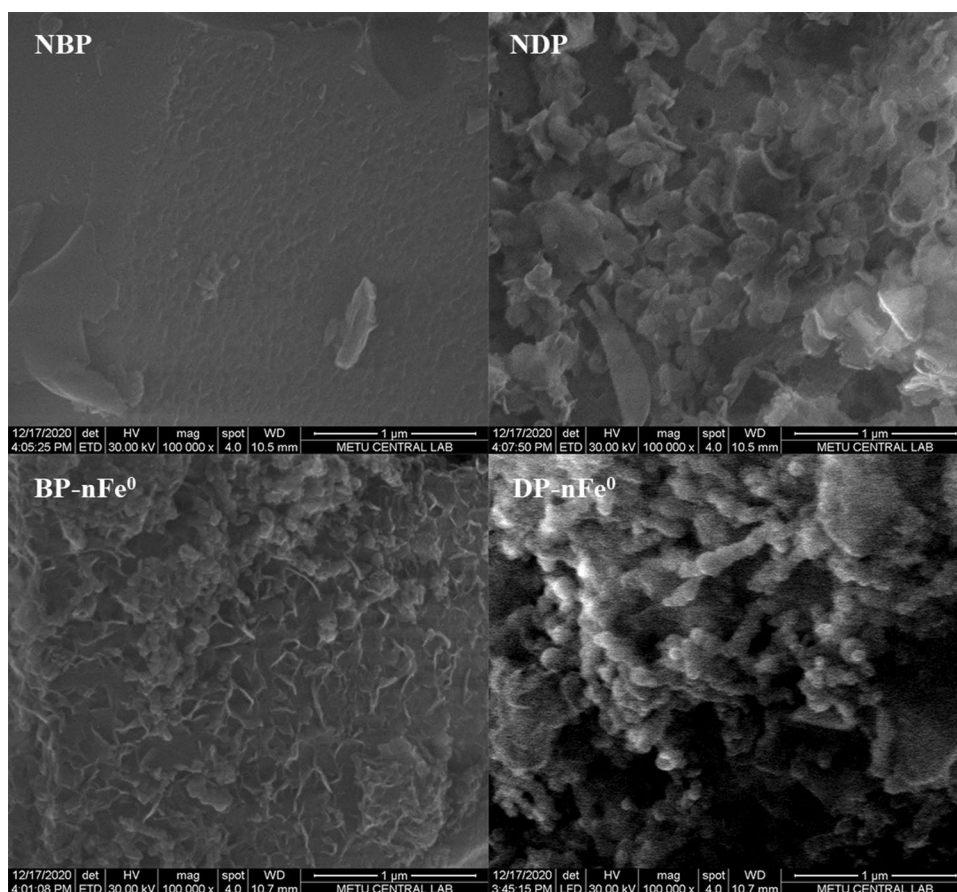**Fig. 1** SEM image of NBP, BP-nFe^0, NDP and DP-nFe^0

Fig. 2 Effect of pH on Cr(VI) removal yield NDP, NBP, DP-nFe^0 and BP-nFe^0 (C$_0$: 50 mg/L; Dose: 0.05 g/10 mL; Temperature: 25 °C; mixing speed: 250 rpm; Time: 30 min). Error bars represent the standard deviation of the measurements

of 1–9 (Fig. 2). Maximum Cr(VI) removal effectiveness was obtained in acidic medium (pH 1–3) for NDP, NBP, DP-nFe^0 and BP-nFe^0 adsorbents. As illustrated in Fig. 2, while pH increased from 1 to 9, adsorption yields of NDP, NBP, DP-nFe^0 and BP-nFe^0 dropped from 54 to 48%, from 57 to 54%, from 95 to 72% and from 74 to 60%, respectively. Both the adsorption and reduction processes of adsorbents were affected by the solution pH value. On the one hand, the adsorption process, caused by electrostatic, hydrophobic and hydrogen bond interactions, is strongly dependent on the solution pH value. On the other hand, pH value determines the current form of Cr(VI). Below pH 6, HCrO$_4^-$ is the dominant species. If the pH rises to above 6, the form shifts to CrO$_4^{2-}$ and Cr$_2$O$_7^{2-}$, and when pH > 7.5, CrO$_4^{2-}$ is the only existence of chromate (Lv et al. 2012). On the other hand, pH value determines the surface charge of adsorbents. The adsorbent surface is highly protonated in an acidic solution medium. It increases the attraction force between positively charged adsorbent surface and negatively charged anionic species HCrO$_4^-$ (Zhang et al. 2012; Xu et al. 2018). In addition, the reduction process of Cr(VI) (expressed as Eqs.(1)) by nFe^0 was also affected by pH value. From this equation, it was easier to find out that H$^+$ is strongly needed and consumed all along the reaction (Lv et al. 2012). That explained why an acidic environment is preferred by the removal of Cr(VI) in aqueous solution by nFe^0.

$$2HCrO_4^- + 3Fe^0 + 14H^+ \rightarrow 3Fe^{2+} + 2Cr^{3+} + 8H_2O \qquad (1)$$
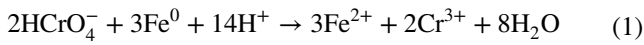
This phenomenon can be seen as another reason for the low Cr(VI) ions concentration found by 1,5-diphenylcarbazide method during analysis. Increasing the pH of the solution reduces the degree of positive charge on the adsorbent and leads to poor attachment of negative species to the adsorbent surface. The other negative ion OH^- in the basic medium can contend with the main anion CrO_4^{2-} ions for adsorption on the adsorbents (Qin et al. 2020; Wu et al. 2020). Since the highest Cr(VI) removal is obtained at acidic pH and the real Cr(VI) solutions are also acidic, pH correction is not required in the practical applications of NDP, NBP, DP-nFe^0 and BP-nFe^0 adsorbents. Similar results of various adsorbents have been reported to remove chromium using pumice. Sepehr et al. (Sepehr et al. 2014) examined

the effect of pH in the range of 1–9 for the removal of chromium ions with native pumice (NP) and modified pumice (MGMP). They have shown that chromium sorption is pH dependent using NP and MGMP and higher extraction efficiency is observed at pH 2.

Initial Cr(VI) concentration-contact time profile modeling

Figure 3a–d shows the effect of initial Cr(VI) ion concentration and contact time on the removal effectiveness of Cr(VI) onto NDP, NBP, DP-nFe^0 and BP-nFe^0 adsorbents. As can be seen, the intake of Cr(VI) in initial phase was high for each of the four adsorbents with a higher adsorption rate. An interesting feature of an adsorbent is that it adsorbs the solute rapidly in the first stage. Removal of Cr(VI) ions increased as the contact time increased until reaching
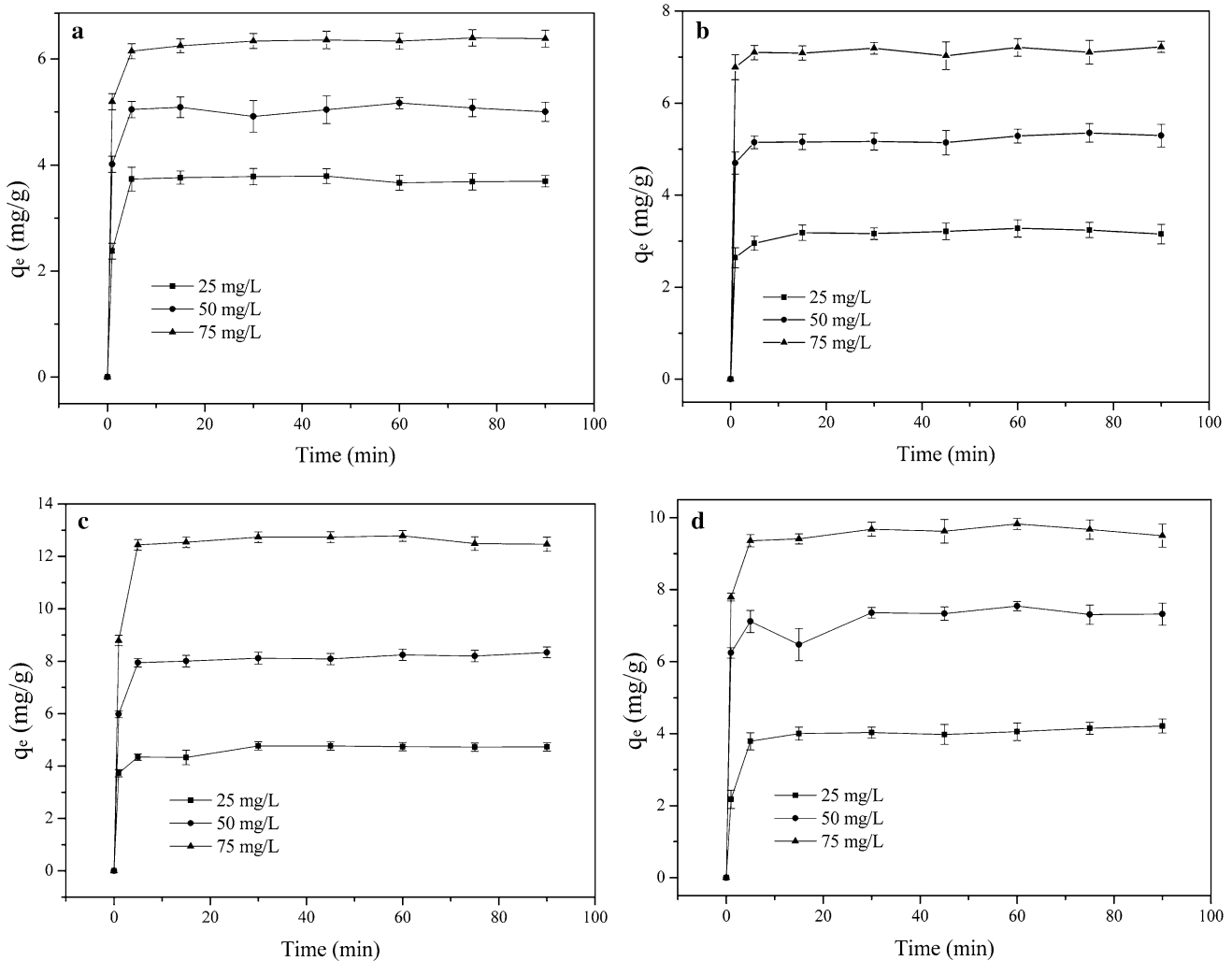

Fig. 3 Influence of contact time and initial chromium concentration on the removal efficiency of **a** NDP, **b** NBP, **c** DP-NFe^0, **d** BP-nFe^0 (pH: 2, adsorbent: 0.05 g/L, 25 °C temperature and 250 rpm agitation speed). Error bars represent the standard deviation of the measurements

equilibrium, because after about 20 min, the removal of chromium did not change significantly and was therefore taken into account thereafter. After 20 min contact time, 3.8, 4.9, 6.2 mg Cr(VI)/g NDP, 3.1, 5.2, 7.2 mg Cr(VI)/g NBP, 4.8, 8.1, 12.8 mg Cr(VI)/g DP-nFe^0 and 3.7, 6.9, 9.4 mg Cr(VI)/g BP-nFe^0 have been removed for 25, 50, 75 mgL^{-1} initial Cr (VI) concentrations, respectively. In the current study, as the chromium concentration increases, the removal efficiency of the chromium increases in certain adsorbent mass (Zhou et al. 2020; Yu et al. 2020).

Effect of adsorbent dosage

Figure 4 demonstrates the effect of adsorbent's dosage on the removal efficacy of Cr(VI) onto NDP, NBP, DP-nFe^0 and BP-nFe^0 at the room temperature. From the curves in Fig. 2, you can easily see that the adsorption capacity (q_e) decreases as the amount of adsorbent increases. This is due to the fact that the active areas on the absorbent surface are not saturated by Cr(VI) ions. As the Cr(VI) concentration is constant and the amount of adsorbent increases, the Cr(VI) concentration decreases compared to the amount of adsorbent in the aqueous medium. Hence, the adsorbent is contacted with less Cr(VI) ions, that is, its active sites in the adsorbent remain unsaturated, meaning that the active sites remain unsaturated in the adsorbent. Thus, there has been a decrease in the adsorption value. In addition, as the amount of adsorbent increases, it increases in stacking and aggregation. This phenomenon increases the total amount of surface overlap of the absorbent material, and the active specific surface areas are reduced for absorption. This restricts the absorption capacity. Active specific surface sites for

Fig. 4 Effect of NDP, NBP, DP-nFe^0 and BP-nFe^0 mass on chromium removal (Cr(VI) concentration = 50 mg/L, contact time 60 min, pH 2, 25 °C temperature and 250 rpm agitation speed)

adsorption were found to be unsaturated with adsorption (Gupta and Babu 2009; Jain et al. 2010; Sepehr et al. 2014).

Measurement of adsorption isotherm

The adsorption isotherms of the of NDP, NBP, DP-nFe^0 and BP-nFe^0 were investigated by 1,5-diphenylcarbazide spectrophotometric method. In our experiment, 50 mg of NDP, NBP, DP-nFe^0 and BP-nFe^0 was incubated with solutions of different Cr(VI) concentrations (from 20 to 100 mg/L, pH = 2) at 25 °C. Langmuir, Freundlich, Dubinin–Radushkevich (DR), Temkin and Jovanoic (Rangabhashiyam et al. 2014) were utilized to describe Cr(VI) adsorption isotherms to detect adsorbent surface properties and adsorption capacity of NDP, NBP, DP-nFe^0 and BP-nFe^0. The Langmuir isotherm model was established using the following equation (Langmuir 1918; Tural et al. 2017):

$$q_e = \frac{q_{\max} K_L C_e}{1 + K_L C_e} \tag{2}$$

where q_e (mg/g), C_e (mg/L) and $q_{\max}$ (mg/g) are the amounts of Cr(VI) bound to the NBP, BP-nFe^0, NDP and DP-nFe^0 adsorbents, the free concentration of Cr(VI) at adsorption equilibrium and the maximal adsorption capacity of the adsorbents, respectively. K_L is the Langmuir constant related to the adsorption capacity (L/mg). The equilibrium constants for these models were determined using linear regression analysis. The necessary properties of the Langmuir isotherm model are expressed as the equilibrium parameter, the dimensionless constant R_L is referred as the separation/equilibrium parameter. R_L is the separation factor expressed as

$$R_L = \frac{1}{1 + K_L C_0} \tag{3}$$

if $R_L > 1$, the adsorption is unfavorable; if $R_L = 1$, linear; if $0 < R_L < 1$, favorable; if $R_L = 0$, irreversible. The Cr(VI) adsorption equilibrium data of NBP, BP-nFe^0, NDP and DP-nFe^0 adsorbents are compatible with the Langmuir model and results are shown in Table 2. The maximum adsorption capacity q_m values of NBP, BP-nFe^0, NDP and DP-nFe^0
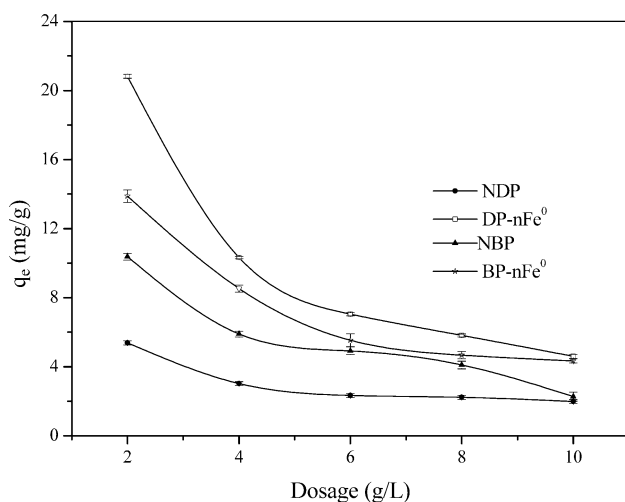
Table 2 Langmuir separation factor for NBP, BP-nFe^0, NDP, DP-nFe^0

Initial Cr(VI) concentration (mg/L)	R_L value			
	NBP	BP-nFe^0	NDP	DP-nFe^0
20	0.361	0.416	0.099	0.907
40	0.220	0.263	0.052	0.830
60	0.159	0.192	0.035	0.765
80	0.124	0.151	0.027	0.709
100	0.102	0.125	0.021	0.661

were 10.82 mg/g, 14.30 mg/g, 17.39 mg/g and 161.29 mg/g for, respectively (Table 3). DP-nFe^0 adsorbent offered superior adsorption capacity compared to NBP, BP-nFe^0 and NDP adsorbents. The experimental data fitting the Langmuir model give a linear plot of NBP, BP-nFe^0, NDP and DP-nFe^0 adsorbents. Coefficient of determination (R^2) was in range of 0.981, 0.959, 0.991, 0.994 for NBP, BP-nFe^0, NDP and DP-nFe^0 adsorbents, respectively. The R_L values decreased with increasing Cr(VI) concentration from 0.021 to 0.361 for NDP and NBP adsorbents, and BP-nFe^0 and DP-nFe^0 adsorbents range between 0.125 and 0.907 results (Table 2) Using the adsorbents studied, the Cr(VI) supported. The R_L values were found decreasing with increasing Cr(VI) concentration for NDP and NBP adsorbents range from 0.021 to 0.361, and BP-nFe^0 and DP-nFe^0 adsorbents range between 0.125 and 0.907. As can be seen from Table 2, the results obtained from Cr(VI) removal with NBP, BP-nFe^0, NDP and DP-nFe^0 adsorbents favored the adsorption process.

Freundlich isotherm model expression proposing multilayer adsorption is an empirical equation based on the heterogeneous surface area of adsorption (Freundlich and Helle 1939; Freundlich 1907). The Freundlich isotherm model is established using the following equation:

$$q_e = K_F C_e^{1/n_F} \tag{4}$$

where q_e (mg/g) and C_e (mg/L) are the amounts of Cr(VI) bound to the NBP, BP-nFe^0, NDP and DP-nFe^0 at adsorption equilibrium and the free concentration of Cr(VI) at adsorption equilibrium, respectively. K_F and n_F are the

Freundlich constants related to the adsorption capacity and intensity, respectively. The equilibrium constants for these models were determined using linear regression analysis. If the value of n_F ranges between 1 and 10, indicate favorable adsorption. The value of nF for NBP, BP-nFe^0, NDP and DP-nFe^0 was 8.08, 1.84, 1.23 and 1.01, respectively. This reveals that $1/n_F$ less than 1 signifies that use of adsorbents favored Cr(VI) adsorption. The coefficient of determination value of NBP (0.939) is lower compared to the BP-nFe^0 (0.962), NDP (0.968) and DP-nFe^0 (0.967) adsorbents.

Dubinin–Radushkevich isotherm model defines the porous structure of NBP, BP-nFe^0, NDP and DP-nFe^0 adsorbents. This model is based on adsorption potential theory, based on the assumption that adsorption is related to microporous filled adsorbate into the adsorbent, and not the layer-by-layer on pore walls (Dubinin and Radushkevich 1947). The linear presentation of the D-R isotherm equation is expressed by

$$q_e = q_{\max}{}^{\exp\left(-\beta\varepsilon^2\right)} \tag{5}$$

$$\varepsilon = RT \ln\left(1 + \frac{1}{C_e}\right) \tag{6}$$

where q_e is the amount of Cr(VI) adsorbed on per unit weight of materials (mg/g), $q_{\max}$ is the maximum adsorption capacity (mg/g), β is the activity coefficient related to the mean free energy of adsorption (mol^2/J^2) and ε is the Polanyi potential. R is universal gas constant (8.314 J/mol K), T is kelvin temperature (K) and mean adsorption energy E (kJ/mol).

$$E = \frac{1}{\sqrt{2\beta}} \tag{7}$$

Mean adsorption energy E (kJ/mol) displays important information about the nature of adsorption process. The E values in the range from 8 to 16 kJ/mol indicate chemical mechanism. If the E value is less than 8 kJ/mol, it indicates physical adsorption. The values of $q_{\max}$ and β given in Table 3 were obtained from the graph of log qe versus ε^2 for the NBP, BP-nFe^0, NDP and DP-nFe^0 adsorbents. Great difference in adsorption capacity $q_{\max}$ (mg/g) was observed between the NDP and DP-nFe^0 adsorbents. The DP-nFe^0 adsorbent presented maximum adsorption capacity of 12.86 mg/g. Coefficient of determination R^2 from D-R model is below 0.92 for all adsorbents. Compared to the Langmuir and Freundlich models, the values of R^2 in D-R model were found low. Adsorption energy E (kJ/mol) less than 0.5 for all adsorbents revealed that the Cr(VI) adsorption is driven by physical mechanism (Zaheer et al. 2019).

Temkin isotherm model depends upon temperature, related to Cr(VI) and NBP, BP-nFe^0, NDP and DP-nFe^0

Table 3 Adsorption isotherm parameters for chromium ions on to NBP, BP-nFe^0, NDP ve DP-nFe^0

Isotherms models	Parameters	NBP	BP-nFe^0	NDP	DP-nFe^0
Langmuir	q_m (mg/g)	10.82	14.30	17.39	161.29
	K_L (L/mg)	0.090	0.070	0.008	0.050
	R^2	0.981	0.959	0.991	0.994
Freundlich	K_F (L/g)	2.68	1.51	0.44	0.81
	n_F	8.08	1.84	1.23	1.01
	R^2	0.939	0.962	0.968	0.976
Temkin	b_T (kJ/mol)	2.778	3.776	3.035	7.580
	A_T (L/mg)	0.605	0.473	0.100	0.338
	R^2	0.916	0.935	0.969	0.868
D-R	$q_{\max}$ (mg/g)	8.01	9.903	4.950	12.86
	β (mol^2/J^2)	4×10^{-6}	5×10^{-6}	5×10^{-5}	5×10^{-6}
	E (kJ/mol)	0.353	0.316	0.100	0.316
	R^2	0.823	0.792	0.916	0.859
Jovanovic	K_j (L/g)	−0.025	−0.025	−0.032	−0.104
	$q_{\max}$ (mg/g)	3.32	3.95	1.03	2.39
	R^2	0.905	0.822	0.967	0.965

adsorbents surface interaction with all the molecules in the layer of adsorption. Liquid phase adsorption is a complex event, since adsorbed molecules are not organized in identical packed structure (Tempkin and Pyzhev 1940). The nonlinear equation of the Temkin isotherm model is shown as follows:

$$q_e = \frac{RT}{b_T} \ln(A_T C_e) \tag{8}$$

where q_e (mg/g) and C_e (mg/L) were the amount of Cr(VI) bound to the NBP, BP-nFe^0, NDP and DP-nFe^0 and the free concentration of Cr(VI) at adsorption equilibrium. A_T is the equilibrium bond constant related to the maximum energy of bond, b_T (kJ/mol) is the Temkin constant concerned with the adsorption heat. R (8.314 kJ/mol K) is the universal gas constant, and T is the Kelvin temperature. The determined values of the Temkin isotherm model constants are shown in Table 3. The b_T constant of Temkin model was obtained within range of 2.77–7.58 kJ/mol, and A_T Temkin constant 0.10–0.60 L/mg, for adsorbents. Coefficient of determination $R^2 \geq 0.868$ is found for all adsorbents.

Jovanovic isotherm model assumptions are similar to the Langmuir model, which is used to predict monolayer localized adsorption without lateral interaction. This model applies to mobilized and localized phase adsorption during high solute concentrations reaching the saturation level (Jovanovic 1969). The nonlinear equation of the Jovanovic isotherm model is shown as follows:

$$q_e = q_{\max}(1 - e^{K_j C_e}) \tag{9}$$

where K_j (L/g) and $q_{\max}$ (mg/g) are the Jovanovic isotherm constant and the maximum adsorption capacity, respectively, in Jovanovic model. The calculated constants from the linear equation of the Jovanovic isotherm model are shown in Table 3. When the adsorption capacities of the isotherm models are compared, it was seen that adsorption capacity of The Jovanovic model is lower than that of the other isotherm models. R^2 value of NDP (0.967) and DP-nFe^0 (0.965) is greater than that of NBP (0.905) and BP-nFe^0 (0.822).

Measurement of adsorption kinetics

The kinetic model data help to evaluate the rate determining step of Cr(VI) adsorption by NBP, BP-nFe^0, NDP and DP-nFe^0 adsorbents. Four kinetic models, pseudo-first-order, pseudo-second-order, Elovich model and intraparticle diffusion models, were used to analyze the experimental data and examine the adsorption kinetics (Alberti et al. 2012).

The pseudo-first-order equation was given by Lagergren and this model applicable during the initial stage of the adsorption process (Lagergren 1898). The equation of the nonlinear pseudo-first-order model is presented as follows:

$$\log(q_e - q_t) = \log q_e - \frac{k_1 t}{2.303} \tag{10}$$

where q_e and q_t (mg/g) represent the adsorption capacities at equilibrium time and time t (min), and k_1 (1/min) is adsorption rate constant of nonlinear pseudo-first-order model. The results of the pseudo-first-order kinetic model parameter of adsorbents such as NBP, BP-nFe^0, NDP and DP-nFe^0 toward the removal of Cr(VI) are presented in Table 4. The pseudo-first-order rate constant is obtained from the slope of plot between log (q_e–q_t) against time, t.

The equation of the nonlinear pseudo-second-order model (Ho and McKay 1999) is presented as follows:

$$\frac{t}{q_t} = \frac{1}{k_2 q_e^2} + \frac{1}{q_e} t \tag{11}$$

where q_e and q_t (mg/g) represent the adsorption capacity at equilibrium time and time t (min), respectively, and k_2 (g/mg min) is the adsorption rate constant of the nonlinear pseudo-second-order model. The experimental data analysis of Cr(VI) adsorption using NBP, BP-nFe^0, NDP and DP-nFe^0 adsorbents showed better fitness with the pseudo-second-order kinetic model. The values of k_2 and q_e calculated from the pseudo-second-order equation are shown in Table 4. The values of R^2 showed that the pseudo-second-order model best fitted the Cr(VI) adsorption behavior of NBP, BP-nFe^0, NDP and DP-nFe^0 adsorbents, indicating that the adsorption is the rate-controlling step. R^2 values obtained from the pseudo-second-order kinetics model are found higher compared to the pseudo-first-order isotherm model.

The intraparticle diffusion model was used to determine the diffusion mechanism (Weber and Morris 1962). The kinetic expression of the model was established using the following equation:

$$q_t = k_{\text{int}} t^{0.5} + C \tag{12}$$

where k_{int} (mg/g min$^{0.5}$) and C (mg/g) are the rate constant and the intercept, respectively. Informative information about the boundary layer thickness of the diffusion mechanism of adsorption is obtained by the expression of the intraparticle diffusion model. The values of k_{int} and C calculated from the intraparticle diffusion equation are shown in Table 4.

It is understood from the the R^2 values that the experimental data are not well defined according to the intraparticle diffusion model. The value of intercept C was observed in the range of 1.401–26.839 for all adsorbents.

The Elovich model (Wu et al. 2009) explains that adsorption performance is related to chemical adsorption and heterogeneous systems. The kinetic model is established using the following equation (Wu et al. 2009)

Table 4 Pseudo-first-order and pseudo-second-order kinetic modeling constants of NBP, BP-nFe⁰, NDP and DP-nFe⁰

Adsorbent	C_0 (mg/L)	q_{exp} (mg/g)	Pseudo-first-order			Pseudo-second-order			Intraparticle			Elovich		
			k_1 (1/min)	q_e (mg/g)	R^2	k_2 (g/mg min)	q_e (mg/g)	R^2	k_{int} (mg/g min0.5)	C (mg/g)	R^2	α (mg/g min)	β (g/mg)	R^2
NBP	25	3.183	0.695	0.472	0.996	3.735	3.209	0.999	0.055	2.795	0.635	3.38×10^9	7.980	0.863
	50	5.158	1.145	2.956	0.956	0.370	5.327	0.999	0.054	4.853	0.667	9.10×10^{17}	8.584	0.815
	75	7.088	0.960	2.686	0.839	0.701	7.189	0.999	0.033	6.908	0.490	1.34×10^{40}	13.514	0.656
BP-nFe⁰	25	4.040	0.573	3.642	0.995	0.272	4.189	0.999	0.102	3.937	0.723	411.87	2.644	0.779
	50	7.370	1.509	4.188	0.981	0.311	7.402	0.999	0.862	23.793	0.879	5.88×10^{11}	4.130	0.650
	75	9.409	0.997	6.695	0.977	7.710	9.625	0.999	1.075	26.839	0.906	2.87×10^{10}	2.762	0.753
NDP	25	1.888	1.007	1.934	0.999	−5.901	1.852	0.999	0.127	0.937	0.470	6.730	8.097	0.583
	50	2.546	0.783	1.820	0.962	5.649	2.519	0.999	0.155	1.401	0.408	4.21×10^{11}	11.261	0.618
	75	3.132	0.746	1.991	0.935	1.279	3.199	0.999	0.199	1.748	0.425	1.87×10^{11}	8.591	0.793
DP-nFe⁰	25	4.330	1.428	3.447	0.995	0.575	4.757	0.999	0.102	3.937	0.723	5.92×10^8	4.460	0.895
	50	8.004	0.962	6.662	0.993	0.205	8.319	0.999	0.862	23.793	0.880	1.64×10^8	2.315	0.761
	75	12.474	0.937	11.127	0.996	0.739	12.547	0.999	1.080	26.839	0.906	1.38×10^8	1.467	0.676

$$q_t = \frac{1}{\beta} \ln(\alpha\beta) + \frac{1}{\beta} \ln(t) \tag{13}$$

The constant α (mg/g min) is related to the rate of chemisorption, and the constant β (g/mg) is related to the surface coverage. Elovich kinetic model parameters are obtained from the plot of q_t versus $\ln(t)$ via slope and intercept. The values of R^2 showed that the experimental data are not well described by Elovich model (Table 4).

Mechanism of Cr(VI) removal

A two-step interaction mechanism is proposed (Fu et al. 2016; Lv et al. 2012; Ullah et al. 2020). In the beginning, Cr(VI) in aqueous solution was absorbed on the BP-nFe⁰ and DP-nFe⁰ surface (Fu et al. 2016; Lv et al. 2012; Ullah et al. 2020). Then, Cr(VI) was reduced by nFe⁰ and coprecipitated or precipitated on the surface of BP-nFe⁰ and DP-nFe⁰ material. The removal of Cr(VI) using BP-nFe⁰ and DP-nFe⁰ adsorbents was extremely rapid at the first 5 min, indicating an initial adsorption in this reaction. Moreover, from the kinetic study data using the so-called second-order adsorption model, it can be concluded that the rate control step is most likely adsorption rather than reduction. In addition, the adsorption ability and stability of pumice were crucial for improving Cr(VI) removal. The pumice surface provided numerous reactive sites to capture Cr(VI), and the adsorbed Cr(VI) enhanced the transfer of floating electrons on the pumice surface, which accelerated the electron transfer from nFe⁰ to Cr(VI) (Fu et al. 2016; Lv et al. 2012; Ullah et al. 2020).

Conclusion

In this study, pumice from different regions in Turkey (Diyarbakir; NDP and Bitlis; NBP) structurally was characterized by BET, XRF, SEM and EDX. Synthesis of nFe⁰ was performed under the same conditions using both NDP and NBP as support materials. Iron content of NBP, NDP, DP-nFe⁰ and BP-nFe⁰ was obtained from EDX analysis. According to the EDX results, the percentage of zero-valent iron is affected when pumice obtained from different regions of Turkey was used as support material. Iron content, which was 1.99% in NBP, increased 1.9-fold after synthesis to 3.83%. However, iron content of NDP (2.08%) increased approximately 29 times after synthesis (60%). NDP, NBP, DP-nFe⁰ and BP-nFe⁰ have been used to remove Cr(VI). In order to optimize reaction parameters, it was aimed to find the most effective conditions by changing the initial Cr(VI) concentration, contact time, adsorbent amount and pH values. The removal of Cr(VI) on this system was strongly pH dependent, and the reaction between Cr(VI) and NDP, NBP,

DP-nFe^0 and BP-nFe^0 adsorbents followed pseudo-second-order kinetics. The adsorption isotherm results fitted well with Langmuir models, and the maximum adsorption capacity of Cr(VI) was 10.82, 14.30, 161.29 and 17.39 mg/g for NDP, NBP, DP-nFe^0 and BP-nFe^0 adsorbents, respectively, at pH 2.0 and 25 °C. The results showed that NDP is a much better support material for nano-zero-valent iron when compared to NBP pumice.

Compliance with ethical standards

Conflict of interest The authors declare that they have no conflict of interest.

References

Alam MM, Alothman ZA, Naushad M, Aouak T (2014) Evaluation of heavy metal kinetics through pyridine based Th(IV) phosphate composite cation exchanger using particle diffusion controlled ion exchange phenomenon. J Ind Eng Chem 20(2):705–709

Alberti G, Amendola V, Pesavento M, Biesuz R (2012) Beyond the synthesis of novel solid phases: review on modelling of sorption phenomena. Coord Chem Rev 256(1–2):28–45

Alothman ZA, Naushad M, Ali R (2013) Kinetic, equilibrium isotherm and thermodynamic studies of Cr(VI) adsorption onto low-cost adsorbent developed from peanut shell activated with phosphoric acid. Environ Sci Pollut Res 20(5):3351–3365

Amin M, Hashem F, El-Gamal S (2018) Utilization of OPC-pumice composites for efficient heavy metals removal. J Taibah Univ Sci 12:765–773

Dalal U, Reddy SN (2019) A novel nano zero-valent iron biomaterial for chromium (Cr^{6+} to Cr^{3+}) reduction. Environ Sci Pollut Res 26:10631–10640

Deng Y-Y, Xiao X-F, Wang D, Han B, Gao Y, Xue J-L (2020) Adsorption of Cr(VI) from aqueous solution by ethylenediaminetetraacetic acid-chitosan-modified metal-organic framework. J Nanosci Nanotechnol 20:1660–1669

Derakhshan Z, Baghapour MA, Ranjbar M, Faramarzian M (2013) Adsorption of methylene blue dye from aqueous solutions by modified pumice stone: kinetics and equilibrium studies. Sci Inform Database 2(3):136–144

Dubinin MM, Radushkevich LV (1947) Evaluation of microporous materials with a new isotherm. Dokl Akad Nauk SSSR 55:331–334

Freundlich H (1907) Über die adsorption in lösungen. Z Phys Chem 57:385–470

Freundlich H, Helle W (1939) On adsorption in solution. J Am Chem Soc 61:2228–2230

Fu P, Wang F, Ma L, Yang X, Wang H (2016) Fine particle sorting and classification in the cyclonic centrifugal field. Sep Purif Technol 158:357–366

Guler UA, Cebeci MS (2017) Potential of pumice modified with iron(III) for copper removal from aqueous solutions. Environ Protect Eng 43

Gupta S, Babu B (2009) Removal of toxic metal Cr(VI) from aqueous solutions using sawdust as adsorbent: equilibrium, kinetics and regeneration studies. Chem Eng J 150:352–365

Harman B, Ibrahim N (2018) Competitive Adsorption of Heavy Metals from Water Using Pumice Supported Nanoscale Zero-Valent Iron. In: Special Issue of the 7th International Advances in Applied Physics and Materials Science (APMAS 2017), vol 134, pp 171–173

Ho YS, McKay G (1999) Pseudo-second order model for sorption processes. Process Biochem 34(5):451–465

Huang X, Liu Y, Liu S, Tan X, Ding Y, Zeng G, Zhou Y, Zhang M, Wang S, Zheng B (2016) Effective removal of Cr(VI) using β-cyclodextrin–chitosan modified biochars with adsorption/reduction bifunctional roles. RSC Adv 6:94–104

Indah S, Helard D, Marchelly F, Putri DE (2018) Adsorption and regeneration of indonesian natural pumice for total chromium removal from aqueous solution indonesian. J Environ Manag Sustain 2:30–37

Jain M, Garg VK, Kadirvelu K (2010) Adsorption of hexavalent chromium from aqueous medium onto carbonaceous adsorbents prepared from waste biomass. J Environ Manag 91:949–957

Jiang D, Huang D, Lai C, Xu P, Zeng G, Wan J, Tang L, Dong H, Huang B, Hu T (2018) Difunctional chitosan-stabilized Fe/Cu bimetallic nanoparticles for removal of hexavalent chromium wastewater. Sci Total Environ 644:1181–1189

Jonasi V, Matina K, Guyo U (2017) Removal of Pb(II) and Cd(II) from aqueous solution using alkaline-modified pumice stone powder (PSP): equilibrium, kinetic, and thermodynamic studies. Turk J Chem 41:748–759

Jovanović DS (1969) Physical adsorption of gases. Kolloid-Zeitschrift Und Zeitschrift Für Polym 235(1):1214–1225

Lagergren SK (1898) About the theory of so-called adsorption of soluble substances. Sven Vetenskapsakad Handingarl 24:1–39

Langmuir I (1918) The adsorption of gases on plane surfaces of glass, mica and platinum. J Am Chem Soc 40:1361–1403

Li J, Zhou Q, Liu Y, Lei M (2017) Recyclable nanoscale zero-valent iron-based magnetic polydopamine coated nanomaterials for the adsorption and removal of phenanthrene and anthracene. Sci Technol Adv Mater 18(1):3–16

Li M, Mu Y, Shang H, Mao C, Cao S, Ai Z, Zhang L (2020) Phosphate modification enables high efficiency and electron selectivity of nZVI toward Cr(VI) removal. Appl Catal B Environ 263:118364

Liu T, Wang Z-L, Yan X, Zhang B (2014) Removal of mercury(II) and chromium(VI) from wastewater using a new and effective composite: pumice-supported nanoscale zero-valent iron. Chem Eng J 245:34–40

Liu N, Zhang Y, Xu C, Liu P, Lv J, Liu Y, Wang Q (2020) Removal mechanisms of aqueous Cr(VI) using apple wood biochar: a spectroscopic study. J Hazard Mater 384:121371

Luo H, Lin Q, Zhang X, Huang Z, Liu S, Jiang J, Xiao R, Liao X (2019) New insights into the formation and transformation of

active species in nZVI/BC activated persulfate in alkaline solutions. Chem Eng J 359:1215–1223

Lv X, Xu J, Jiang G, Tang J, Xu X (2012) Highly active nanoscale zero-valent iron (nZVI)–Fe_3O_4 nanocomposites for the removal of chromium(VI) from aqueous solutions. J Colloid Interf Sci 369(1):460–469

Periyasamy S, Naushad M, Viswanathan N (2020) Hydrothermal fabrication of triazine-functionalized covalent organic polymer enfolded alginate biocomposite beads for Cr(VI) removal from water. Environ Sci Water Res Technol 6:851–863

Ponder SM, Darab JG, Mallouk TE (2000) Remediation of Cr(VI) and Pb(II) aqueous solutions using supported, nanoscale zero-valent iron. Environ Sci Technol 34(12):2564–2569

Qasim GH, Lee S, Lee G, Lee W, Hong Y, Han S (2018) Dissolved oxygen and nitrate effects on the reduction and removal of divalent mercury by pumice supported nanoscale zero-valent iron. Environ Sci Water Res Technol 4:1651–1661

Qin L, He L, Yang W, Lin A (2020) Preparation of a novel iron-based biochar composite for removal of hexavalent chromium in water. Environ Sci Pollut Res 27:1–13

Rangabhashiyam S, Balasubramanian P (2018) Adsorption behaviors of hazardous methylene blue and hexavalent chromium on novel materials derived from Pterospermum acerifolium shells. J Mol Liquids 254:433–445

Rangabhashiyam S, Balasubramanian P (2019a) The potential of lignocellulosic biomass precursors for biochar production: performance, mechanism and wastewater application-a review. Ind Crops Prod 128:405–423

Rangabhashiyam S, Balasubramanian P (2019b) Characteristics, performances, equilibrium and kinetic modeling aspects of heavy metal removal using algae. Bioresour Technol Rep 5:261–279

Samarghandi MR, Zarrabi M, Amrane A, Soori MM, Sepehr MN (2013) Removal of acid black dye by pumice stone as a low cost adsorbent: kinetic, thermodynamic and equilibrium studies. Environ Eng Manag J (EEMJ) 12

Selvakumar A, Rangabhashiyam S (2019) Biosorption of Rhodamine B onto novel biosorbents from Kappaphycus alvarezii, Gracilaria salicornia and Gracilaria edulis. Environ Pollut 255:113291

Sepehr MN, Amrane A, Karimaian KA, Zarrabi M, Ghaffari HR (2014) Potential of waste pumice and surface modified pumice for hexavalent chromium removal: characterization, equilibrium, thermodynamic and kinetic study. J Taiwan Inst Chem Eng 45:635–647

Shi LN, Zhang X, Chen ZL (2011) Removal of chromium(VI) from wastewater using bentonite-supported nanoscale zero-valent iron. Water Res 45(2):886–892

Shu Y, Ji B, Cui B, Shi Y, Wang J, Hu M, Luo S, Guo D (2020) Almond shell-derived, biochar-supported, nano-zero-valent iron composite for aqueous hexavalent chromium removal: performance and mechanisms. Nanomaterials 10:198

Simeonidis K, Mourdikoudis S, Kaprara E, Mitrakas M, Polavarapu L (2016) Inorganic engineered nanoparticles in drinking water treatment: a critical review. Environ Sci Water Res Technol 2:43–70

Sun Y, Lan J, Du Y, Li Z, Liao X, Du D, Ye H, Zhang TC, Chen S (2020) Efficient removal of heavy metals by synergistic actions of microorganisms and waste molasses. Bioresour Technol 302:122797

Tempkin MI, Pyzhev V (1940) Kinetics of ammonia synthesis on promoted iron catalyst. Acta Phys Chim USSR 12(1):327

Tural B, Ertaş E, Enez B, Fincan SA, Tural S (2017) Preparation and characterization of a novel magnetic adsorbent functionalized with biomass of Bacillus Subtilis: kinetic and isotherm studies of adsorption processes in the removal of methylene blue. J Environ Chem Eng 5:4795–4802

Ullah S, Faiz P, Leng S (2020) Synthesis, mechanism, and performance assessment of zero-valent iron for metal-contaminated water remediation: a review. Clean: Soil, Air, Water 48(9):2000080

Üzüm Ç, Shahwan T, Eroğlu AE, Hallam KR, Scott TB, Lieberwirth I (2009) Synthesis and characterization of kaolinite-supported zero-valent iron nanoparticles and their application for the removal of aqueous Cu^{2+} and Co^{2+} ions. Appl Clay Sci 43(2):172–181

Wang H, Cui H, Song X, Xu R, Wei N, Tian J, Niu H (2020) Facile synthesis of heterojunction of MXenes/TiO_2 nanoparticles towards enhanced hexavalent chromium removal. J Colloid Interf Sci 561:46–57

Weber WJ, Morris JC (1962) Advances in water pollution research. In: Proceedings of the first international conference on water pollution research, vol 2, pp 231

Wu FC, Tseng RL, Juang RS (2009) Characteristics of Elovich equation used for the analysis of adsorption kinetics in dye-chitosan systems. Chem Eng J 150(2–3):366–373

Wu H, Wei W, Xu C, Meng Y, Bai W, Yang W, Lin A (2020) Polyethylene glycol-stabilized nano zero-valent iron supported by biochar for highly efficient removal of Cr(VI). Ecotoxicol Environ Saf 188:109902

Xu C, Yang W, Liu W, Sun H, Jiao C, Lin A-J (2018) Performance and mechanism of Cr(VI) removal by zero-valent iron loaded onto expanded graphite. J Environ Sci 67:14–22

Yu S, Yuan G, Gao H, Liao Y (2020) Removal of Cr(VI) from aqueous solutions using polymer nanotubes. J Mater Sci 55:163–176

Zaheer Z, Bawazir WA, Al-Bukhari SM, Basaleh AS (2019) Adsorption, equilibrium isotherm, and thermodynamic studies to the removal of acid orange 7. Mater Chem Phys 232:109–120

Zhang Y, Li Y, Li J, Sheng G, Zhang Y, Zheng X (2012) Enhanced Cr(VI) removal by using the mixture of pillared bentonite and zero-valent iron. Chem Eng J 185:243–249

Zhang W, Qian L, Ouyang D, Chen Y, Han L, Chen M (2019) Effective removal of Cr(VI) by attapulgite-supported nanoscale zero-valent iron from aqueous solution: enhanced adsorption and crystallization. Chemosphere 221:683–692

Zhou Z, Liu X, Zhang M, Jiao J, Zhang H, Du J, Zhang B, Ren Z (2020) Preparation of highly efficient ion-imprinted polymers with Fe_3O_4 nanoparticles as carrier for removal of Cr(VI) from aqueous solution. Sci Total Environ 699:134334

Zhu N, Xu Y, Dai L, Zhang Y, Hu G (2018) Application of sequential extraction analysis to Pb(II) recovery by zerovalent iron-based particles. J Hazard Mater 351:138–146

مدينة الملك عبدالعزيز
KACST للعلوم والتقنية

Springer